J Electr Eng Technol Vol. 9, No. 1: 106-113, 2014
http://dx.doi.org/10.5370/JEET.2014.9.1.106

ISSN(Print) 1975-0102
ISSN(Online) 2093-7423

Influence of Thermal Expansion on Eccentricity and Critical Speed in Dry Submersible Induction Motors

Qiang Lv*, Xiaohua Bao† and Yigang He*

Abstract – Rotor eccentricity is one of the major factors that directly influence the security of horizontal electrical machines, and the critical speed of the shaft has a close relationship with vibration. This paper deals with the influence of thermal expansion on the rotor eccentricity and critical speed in large dry submersible motors. The dynamic eccentricity (where the rotor is still turning around the stator bore centre but not its own centre) and critical speed of a three-phase squirrel-cage submersible induction motor are calculated via hybrid analytical/finite element method. Then the influence of thermal expansion is investigated by simulation. It is predicted from the study that the thermal expansion of the rotor and stator gives rise to a significant air-gap length decrement and an inconspicuous slower critical speed. The results show that the thermal expansion should be considered as an impact factor when designing the air gap length.

Keywords: Critical speed, Dynamic eccentricity, Submersible motor, Thermal expansion

1. Introduction

In the water conservancy and flood controlling, town sewage treatment or water supply and drainage of industry and mining enterprises, large submersible electric pumps are widely used. In other fields it is also common, such as drilling machines used in bridge construction reconnaissance and thrusters used in submarines or deep-sea exploration ships. All of these subaqueous equipments are usually driven by submersible motors. Some large ones may cost millions of dollars and even more with corollary equipments. However, the reliability of horizontally-installed large submersible motors is still disputable due to the air-gap eccentricity or damageable bearings, etc. This problem not only occurs in large submersible motors, but also in many other kinds of motors. In [1], it has been pointed out that the most important mechanical faults are bearing faults (40%-50%) and eccentricity (60%).

Eccentricity is a condition that unequal air gap exists between the stator and rotor. That leads to a decrement of air-gap length. There are two types of air-gap eccentricity: static eccentricity and dynamic eccentricity. In the case of dynamic eccentricity, the stator symmetrical axis coincides with the rotor rotational axis, but the rotor symmetrical axis displaces. In this case, air-gap distribution is not uniform, and the position of minimum air-gap rotates with the rotor. Generally speaking, there are manifold causes of dynamic eccentricity, such as manufacture tolerances, wear of bearings and incorrect manufacture of the machine components mentioned in [2]. And [3] lists three causes of air-gap eccentricity: 1) manufacturing/installation defect, 2) incorrect positioning of rotor and stator, bent rotor shaft, 3) bearing misalignment, wear, improper lubrication.

Many papers address air-gap eccentricity, including static and dynamic eccentricity. And these papers can be classified in three categories: detection via current condition monitoring or some other methods, vibration generation, and unbalanced magnetic pull (UMP) [4]. Obviously, many studies cover more than one of these areas. Increased losses, as a by-product of rotor eccentricity, are discussed in a few papers. Smith et al [5] described the magnitude of the additional losses in a motor brought about by a progressive increase in the eccentricity of the rotor, and of thus obtaining information as to the amount of eccentricity which may be allowed in practice without serious disadvantages. Papers on the subject of condition monitoring put forward a variety of methods such as finite element method (FEM) [6, 7], artificial neural networks [8], multiple reference frames theory (MRF) [9] and so on. As for eccentricity linked with vibration, some relational papers like [10-12] try to put forward simplified calculation models and focus on the issues with resonant frequencies and the generation of vibrations around the critical speeds.

Although many papers mention eccentricity of electrical machines, few concentrate on the calculation of rotor eccentricity, critical speed and influence of thermal expansion. Dorrell [13] calculated the UMP in small copper (no skew) and aluminum (skewed) cage induction motors with dynamic eccentricity. Wang et al [14] calculated the stiffness and critical speed of magnetic

† Corresponding Author: School of Electrical Engineering and Automation, Hefei University of Technology, P.R. China. (sukz@ustc.edu)
* School of Electrical Engineering and Automation, Hefei University of Technology, P. R. China. (lvqsz@mail.hfut.edu.cn, hyghnu@yahoo.com.cn)
Received: March 19, 2013; Accepted: May 27, 2013

bearing-rotor system based on finite element analysis (FEA), and Yu et al [15] calculated the rotor critical speed from permanent magnet synchronous machine. Furthermore, Belmans [16] analyzed the influence of rotor-bar stiffness on the critical speed of an induction motor, which shows that the generally made approximations for the calculation of the mechanical parameters are no longer acceptable when considering aluminium rotors. Very few papers deal with influence of thermal expansion. Huang [17] pointed out that thermal expansion may lead to extra vibration.

A rational design of air-gap length helps to reduce the probability of failure. Consequently, the authors do research on rotor eccentricity and critical speed from a design perspective. This paper calculates the dynamic eccentricity and critical speed of a rotor in a large dry submersible induction motor via hybrid analytical/finite element method, and meanwhile investigates the influence of thermal expansion on dynamic eccentricity and critical speed.

2. Calculation of eccentricity and critical speed

2.1 Rotation characteristics of shaft

The shaft of a large horizontal submersible motor rotates in a rather complicated way. Actually, the rotor consists of both static eccentricity and dynamic eccentricity. As the shaft is bent due to the gravity, UMP and some other forces, axial-varying rotor eccentricity appears. And bearing faults or assembling error will also result in complicated rotor eccentricity. Fig. 1 illustrates the simplified rotation model of the shaft. The following assumptions are made in this approach.

1) The bearings are rigid bracings.
2) The bearings are manufactured and assembled precisely, or the error is small enough, therefore the axis z in Fig. 1 is just right the geometric centerline of the stator core.
3) The change of temperature does not have significant influence on the physical characteristics of motor materials, so the Young's modulus, Poisson's ratio, thermal expansion coefficient are set as constant.
4) Just taking gravity, UMP and bending stress into consideration. The resultant force provides the centripetal force.
5) The air-gap length is thought to be axially uniform. Hence average rotor eccentricity is used when calculating the UMP.
6) Because of the relatively small deflection of shaft and thermal expansion of the rotor core, the simulation methods are based on linear structural analysis.
7) Average temperature is introduced into the thermal expansion simulation.

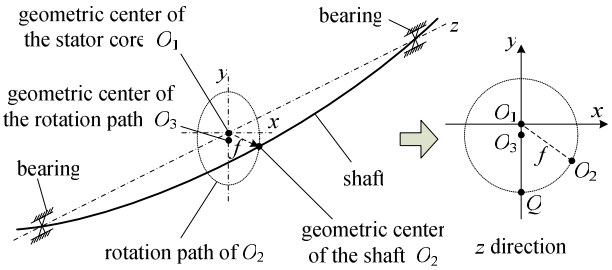

Fig. 1. Rotation model of the shaft

According to the rotor dynamics, the rotation path of the geometric center of a horizontal shaft with rigid bracings is a circle whose center locates at the negative part of axis x, as Fig. 1 shows. The motion state of the shaft belongs to rotary motion which means a rotation state that the centripetal material of the bent shaft is always centripetal, and the internal stress is static stress rather than alternating stress. From the rotation path of O_2 shown in Fig. 1, it can be seen that the maximum eccentricity along the axial direction f will reach the peak at the point Q. This peak value is of interest in this paper because it is the maximum eccentricity during the operation of a submersible motor. It is calculated using hybrid analytical/finite element method.

2.2 Hybrid analytical/finite element method

In order to investigate the influence of thermal expansion on eccentricity and critical speed in submersible induction motors, a hybrid analytical/finite element method is applied in this paper. Fig. 2 shows the flowchart of the method. The eccentricity and critical speed are calculated with both analytical method (AM) and finite element method (FEM). Detailed explanation of each procedure is given later in this section.

To see from a macroscopic perspective, the volumes of the majority of matters increase when heated up, including iron cores in electric machines. As submersible motors usually work under water, the cooling condition of the stator is much better than the rotor especially in dry submersible motors. Then the temperature of the rotor is usually much higher than the stator, and the thermal expansion of the stator is evidently less than that of the rotor. As a result, a decrement in air-gap length is produced.

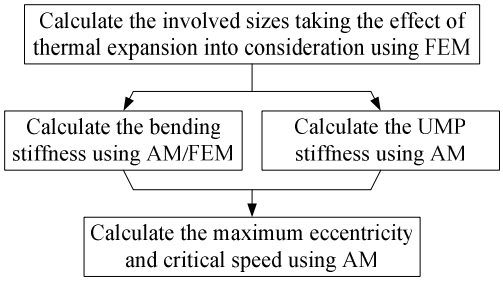

Fig. 2. Flowchart of the hybrid analytical/finite element method

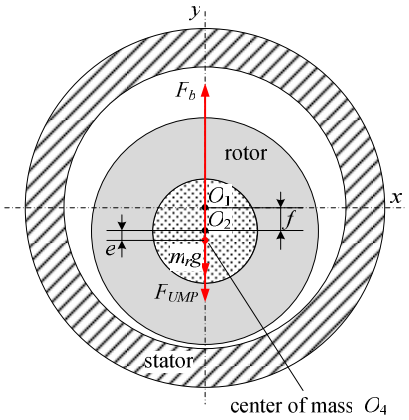

Fig. 3. Cross section of induction motor at point *Q*, including the force condition

The air-gap flux density, bending stiffness and UMP stiffness are calculated considering the thermal expansion.

It has been mentioned that the maximum eccentricity of the shaft at the point *Q* is of interest. Fig. 3 shows the force condition of the rotor at point *Q*. The motion of the rotor can be described as uniform circular motion, and according to Newton's second law of motion, the equation of motion can be expressed as

$$m_r(f+e)\omega^2 = F_b - F_{UMP} - m_r g \tag{1}$$

where m_r is the mass of the rotor, e is the mass eccentricity of the rotor, ω is the angular velocity of the shaft, F_b is the bending stress, F_{UMP} is the UMP, and g is the gravity acceleration. Introducing bending stiffness K and UMP stiffness K_0, Eq. (1) can be represented by

$$m_r(f+e)\omega^2 = Kf - K_0 f - m_r g \tag{2}$$

Then the maximum rotor eccentricity is given by

$$f = \frac{m_r e\omega^2 + m_r g}{K - K_0 - m_r \omega^2} \tag{3}$$

Let the denominator of the right part of Eq. (3) equal to zero, and the critical speed can be calculated from

$$\omega_k = \sqrt{\frac{K - K_0}{m_r}} \tag{4}$$

From the above analysis, it can be seen that the calculation of bending stiffness and UMP stiffness is the key to the successful calculation of eccentricity and critical speed.

The bending stiffness of the shaft can be calculated using either AM or FEM. The differential equation of deflection curve and differential relationship between shearing force, bending moment and load intensity are presented by the following expressions:

$$\frac{dM(z)}{dz} = F_S(z) \tag{5}$$

$$\frac{d^2M(z)}{dz^2} = q(z) \tag{6}$$

$$\left[\frac{d^2 f(z)}{dz^2}\right] \Bigg/ \left\{1 + \left[\frac{df(z)}{dz}\right]^2\right\}^{3/2} = \frac{M(z)}{EI(z)} \tag{7}$$

where $F_s(z)$ is the shearing force, $M(z)$ is the bending moment, $q(z)$ is the load intensity, $f(z)$ is the deflection at the corresponding position of the shaft, E is the Young's modulus of the shaft material and $I(z)$ is the inertia moment of the shaft at the corresponding position. According to Eqs. (5) and (6), the shearing force and bending moment can be expressed as

$$F_S(z) = \int_0^z q(z)dz + C_1 \tag{8}$$

$$M(z) = \int_0^z \int_0^z q(z)dzdz + C_1 z + C_2 \tag{9}$$

where C_1 and C_2 are the integration constants which can be obtained by applying the boundary conditions. In fact, the intersection angle of shaft is generally so small that the magnitude of the term $[df(z)/dz]^2$ is much smaller than 1, therefore Eq. (7) can be simplified as

$$\frac{d^2 f(z)}{dz^2} = \frac{M(z)}{EI(z)} \tag{10}$$

Get (10) integrated twice and the expression of deflection is obtained:

$$f(z) = \int_0^z \int_0^z \frac{M(z)}{EI(z)} dzdz + C_3 z + C_4 \tag{11}$$

where C_3 and C_4 are the integration constants which can be obtained by applying zero and l_s to Eq. (11) where no deflection at this two positions. l_s is the length of the shaft. Finally, the bending stiffness at the center of the shaft is approximately the form

$$K = \frac{\int_0^{l_s} q(z)dz}{f(0.5l_s)}. \tag{12}$$

Another important parameter is the UMP stiffness. The UMP which tries to pull the rotor further off the center can be calculated in traditional formula method. As known to all, the force caused by two electromagnets can be expressed as

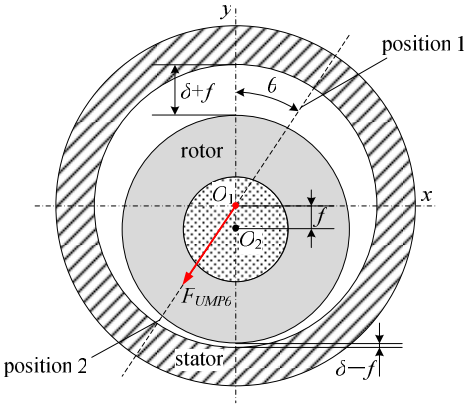

Fig. 4. Illustration of calculating UMP

$$F = \frac{B^2 A}{2\mu_0} \tag{13}$$

where B is the flux density between two electromagnets, μ_0 is the magnetic conductivity in vacuum and A is the area which the flux crosses. According to (13), the UMP produced by one pair of poles is expressed as

$$F_{UMP\theta} = \left[\frac{B_{\delta 2}^2}{2\mu_0} - \frac{B_{\delta 1}^2}{2\mu_0}\right] A_p \tag{14}$$

where A_p is the area of one pole, $B_{\delta 1}$ and $B_{\delta 2}$ are the air-gap flux density at position 1 and 2 shown in Fig. 4. The saturation and the puny change of air-gap coefficient which is caused by the change of air gap length are neglected here. The magnetic motive force of each pole is equivalent:

$$B_{\delta 2}(\delta - e_0 \cos\theta) = B_{\delta 1}(\delta + e_0 \cos\theta) = B_\delta \delta \tag{15}$$

where B_δ is the air-gap flux density when the air gap is uniform, δ is the uniform air-gap length, e_0 is the initial eccentricity, and θ is the angular position. Combine (14) and (15), the UMP leads to the expression

$$F_{UMP} = p\left[\frac{1}{\pi}\int_{-\pi/2}^{\pi/2} F_{UMP\theta}\cos\theta d\theta\right] = p\frac{A_p}{2\mu_0}\frac{4B_\delta^2 e_0}{2\delta} \tag{16}$$

where p is the pole pairs. The area of one pole is denoted by A_p where

$$A_p = \alpha_p' \frac{\pi D}{2p} l_{ef} \tag{17}$$

and α_p' is the calculated pole arc coefficient, D is the inner diameter of the stator, l_{ef} is the calculated length of core. Then the UMP stiffness is given by

$$K_0 = \frac{\beta \pi D l_{ef}}{\delta}\frac{B_\delta^2}{2\mu_0} \tag{18}$$

where β is the empirical coefficient. The signification of the empirical coefficient is the influence of the type of electric machine, distribution of magnetic field, saturation, slots, damping and winding structure. E. Wiedemann [18] gave the value of β in induction motors which is 0.3.

3. Simulation results

A large dry three-phase submersible induction motor is simulated in this section. Finite element simulation is carried out using a finite element-based software ANSYS. Fig. 5 shows the general view of the motor, and specifications of the proposed large dry submersible induction motor have been summarized in Table 1.

The computer simulation results of thermal expansion are shown in Fig. 6. It is carried out by applying the experimental stator temperature to the stator model, and a series of different temperatures to the rotor model. Since the temperature difference of iron core is not very large in submersible motors, average temperature is used in the calculation of thermal expansion. Table 2 lists the experimental results of the stator temperature, including three different positions of the stator core and the average temperature. A large number of experimental results show that the normal operation temperature of the rotor in a submersible motor is between 60˚C and 120˚C. It is quite dangerous when the rotor temperature is higher than 120˚C. Then the rotor temperature is set from 60˚C to 120˚C in the simulation. From the simulation results, it can be seen that the minimum thermal expansion of stator inner radius is 0.06 mm which is located at the center of the stator core;

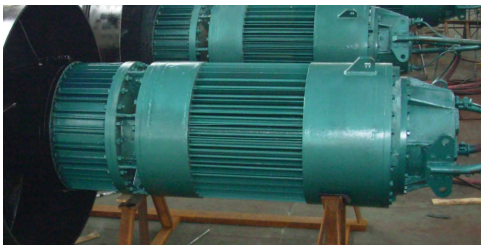

Fig. 5. General view of the large dry submersible induction motor

Table 1. Specifications of the proposed induction motor

Rated power (kW)	800
Rated voltage (V)	10000
Rated frequency (Hz)	50
Number of phases	3
Number of pole pairs	3
Rated speed (rpm)	993
Mean air-gap length (mm)	1.8
Inner diameter of stator (mm)	590
Core length (mm)	700
Air-gap flux density (T)	0.673
Mass of rotor (kg)	1557.9

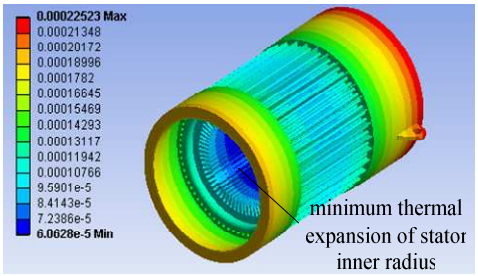

(a) Distribution of stator thermal expansion at 40.1˚C

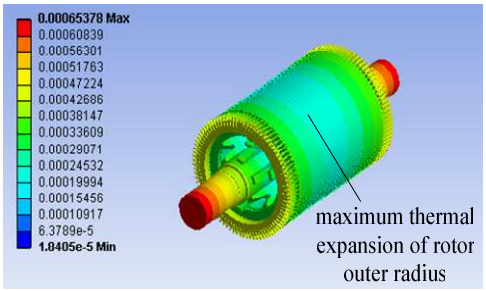

(b) Distribution of rotor thermal expansion

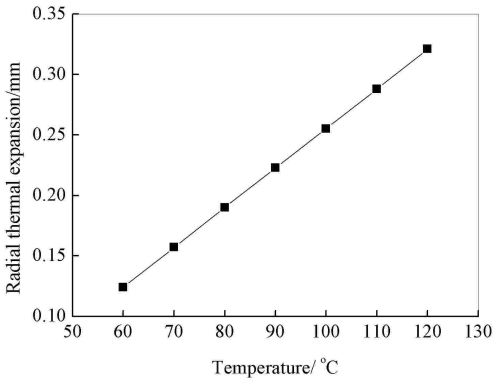

(c) Radial maximum expansion against average temperature of the rotor

Fig. 6. Computer simulation results of thermal expansion

Table 2. Experimental results of the stator temperature

Position	Temperature/˚C	Average Temperature/˚C
Top of stator core	40.2	40.1
Center of stator core	42.4	
Bottom of stator core	37.8	

the maximum thermal expansion of the rotor outer radius located at the center of the rotor core is from 0.124 mm (60˚C) to 0.321 mm (120˚C).

Fig. 7 shows the simulation results of bending stiffness. It is obtained by applying different loads to the shaft between z_1 and z_2, as Fig. 7 (a) shows. With small distortion, the eccentricity is thought to be linear and bending stiffness constant. The bending stiffness is approximately 1.24×10^9 N/m.

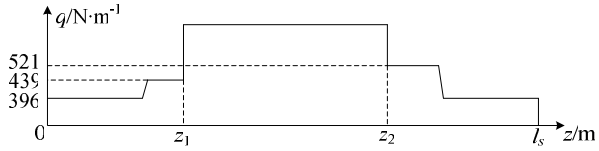

(a) Load distribution along the axis

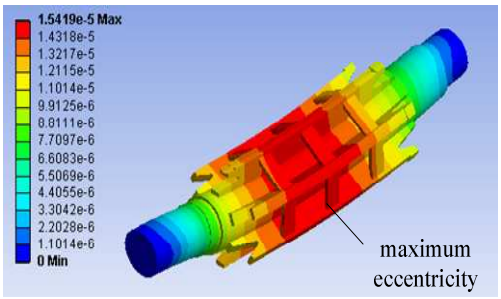

(b) Distribution of shaft eccentricity

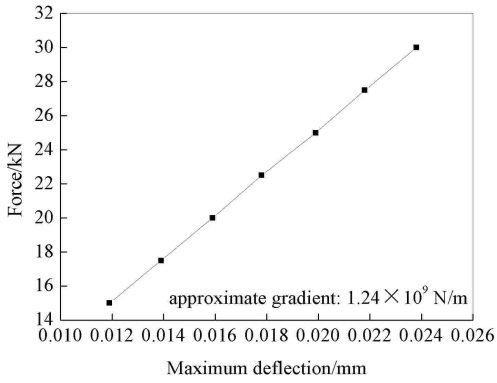

(c) Applied force against dynamic eccentricity

Fig. 7. Simulation results of bending stiffness

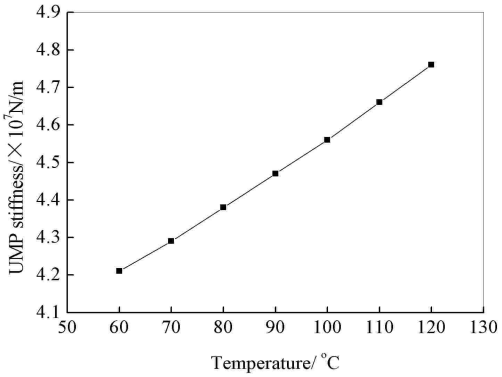

Fig. 8. UMP stiffness variation with rotor temperature

The air-gap flux density B_δ mentioned in Eq. (15) may increase with the decrement of air-gap length, but the magnetizing current decreases due to the higher temperature, and finally the air-gap flux density can be regarded as constant. It can be seen from (18) that the UMP stiffness increases with the expansion of the rotor. Fig. 8 shows the UMP stiffness variation with rotor

temperature.

When the bending stiffness and UMP stiffness are computed, the maximum eccentricity and critical speed are obtained by applying K and K_0 to (3) and (4). The mass eccentricity of rotor can be reflected by $m_r e\omega^2$ in (3), and it is generally reduced to less than 100 g·cm. Because of the UMP stiffness increases with the thermal expansion of the rotor, it is obvious that a larger dynamic eccentricity and a lower critical speed are obtained. Finally, the maximum decrement of air-gap length can be expressed as

$$\delta_{d\max} = f + \delta_E \tag{19}$$

where δ_E is the maximum thermal expansion shown in Fig. 6(c). Considering Eq. (3), the above maximum decrement of air-gap length can be replaced by

$$\delta_{d\max} = \frac{m_r e\omega^2 + m_r g}{K - K_0 - m_r \omega^2} + \delta_E \tag{20}$$

where the bending stiffness K, UMP stiffness K_0, and maximum thermal expansion δ_E are functions of rotor temperature. Fig. 9 shows the variation of maximum decrement of air-gap length with rotor temperature. With the UMP stiffness variation with rotor temperature calculated, the critical speed curve as a function of temperature is easy to obtain. It is shown in Fig. 10. The critical speed without considering thermal expansion is calculated by

$$\omega_k' = \sqrt{\frac{K - K_0'}{m_r}} \tag{21}$$

where K_0' is the UMP stiffness without considering thermal expansion.

Practice shows that in order to ensure the safe and reliable operation of an electric motor, the smaller the air gap decrement of an induction motor is, the better, and the critical speed should be at least 30% faster than the rated speed. If the thermal expansion is not considered, the decrement of air gap is 0.7% and the critical speed is 844.3% faster than the rated speed. However, it can be seen from the simulation results that the air gap decrement increases from 4.3% (60˚C) to 15.2% (120˚C) and the critical speed decreases from 850.3% (60˚C) to 848.3% (120˚C) faster than the rated speed when considering the influence of temperature (thermal expansion). Therefore, the influence of thermal expansion should be considered when designing the shaft.

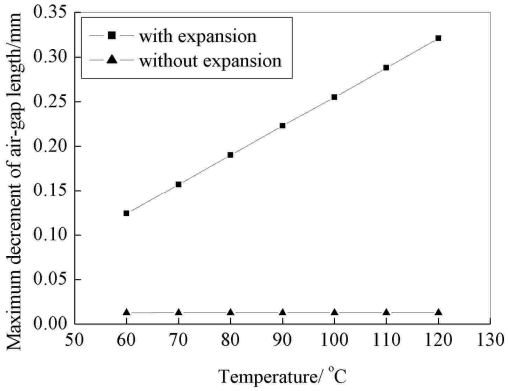

Fig. 9. Variation of maximum decrement of air-gap length with rotor temperature

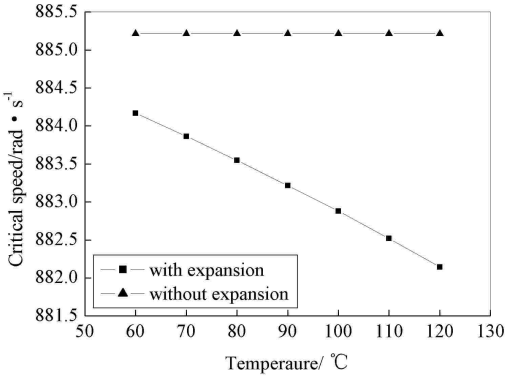

Fig. 10. Variation of critical speed with rotor temperature

4. Conclusions

The hybrid analytical/finite element method is used to calculate the dynamic eccentricity and the critical speed of a large dry submersible induction motor, considering the influence on thermal expansion of both the rotor and stator. This study shows that the thermal expansion of the rotor and stator makes the minimum air gap of dynamic eccentricity smaller and the critical speed slower. The simulation results indicate that the thermal expansion is not small enough to be neglected compared with the air-gap length. The thermal expansion of the rotor is a more important factor that leads to the smaller minimum air gap than stator thermal expansion. Nevertheless, the thermal expansion may not have much influence on the critical speed of the rotor, if the bending stiffness is large enough. Thus the thermal load and design of rotor cooling system is important in order to limit the thermal expansion in case a stator and rotor rub in horizontal dry submersible motors.

Acknowledgements

This work was supported by the National Natural Science Funds of China for Distinguished Young Scholar (No. 50925727), the National Natural Science Funds of China (No. 51177033), Fundamental Research Funds for the Central Universities (2012HGZY 0003) and Hefei Hengda Jianghai Pump Co; Ltd.

References

[1] J. Faiz, B. M. Ebrahimi, B. Akin, and H. A. Toliyat, "Finite-element trainsient analysis of induction motors under mixed eccenrticity fault," *IEEE Transactions on Magnetics*, Vol. 44, No. 1, pp. 66-74, Jan. 2008.

[2] G. M. joksimovic, M. D. Durovic, J. Penman, and N. Arthur, "Dynamic simulation of dynamic eccentricity in induction machines-winding function approach," *IEEE Transactions on Energy Conversion*, Vol. 15, No. 2, pp. 143-148, Jun. 2000.

[3] D. Basak, A. Tiwari, and S. P. Das, "Fault diagnosis and condition monitoring of electrical machines-A review," *IEEE Internatinal Conference on Industrial Technology*, pp. 3061-3066. Dec. 2006.

[4] D. G. Dorrell, "Sources and characteristics of unbalanced magnetic pull in three-phase cage induction motors with axial-varying rotor eccentricity," *IEEE Transactions on industry Applicatinos*, Vol. 47, No. 1, pp. 12-24, Jan/Feb. 2011.

[5] Charles F. Smith, and Eric M. Johnson, "The losses in induction motors arising from eccentricity of the rotor," *Journal of the Institution of Electrical Engineers*, Vol. 48, No. 212, pp. 546-569, 1921.

[6] J. Faiz, B. M. Ebrahimi, B. Akin, and H. A. Toliyat, "comprehensive eccentricity fault diagnosis in induction motors using finite element method," *IEEE Transactions on Magnetics*, Vol. 45, No. 3, pp. 1764-1767. Mar. 2009.

[7] J. Faiz, B. M. Ebrahimi, H. A. Toliyat, and B Akin, "Diagnosis of a mixed eccentricity fault in a squirrel-cage three-phase induction motor using time stepping finite element technique," *IEEE International Conference on Electric Machines & Drives*, Vol. 2, pp. 1446-1450, May. 2007.

[8] D. Matic, F. Kulic, M. Pineda-Sanchez, and J. Pons-Llinares, "Artificial neural networks eccentricity fault detection of induction motor," *IEEE International Multi-Conference on Computing in the Global Information Technology*, pp. 1-4, Sep. 2010.

[9] S. M. A. Cruz, A. J. M. Cardoso, and H. A. Toliyat, "Diagnosis of stator, rotor and airgap eccentricity faults in three-phase induction motors based on the multiple reference frames theory," *IEEE International Conference on Industry Applications*, Vol. 2, pp. 1340-1346, Oct. 2003.

[10] A. Negoita, and R. M. Ionescu, "Influence of rotor static eccentricity on the noise level of a squirrel cage induction motor," *IEEE International Conference on Environment and Electrical Engineering*, pp. 1-4, May. 2011.

[11] J. R. Cameron, W. T. Thomson, and A. B. Dow, "Vibration and current monitoring for detecting airgap eccentricity in large induction motors," *IEEE Proceedings B Electric Power Applications*, Vol. 133, No. 3, pp. 155-163, May. 1986.

[12] D. G. Dorrell, W. T. Thomson, and S. Roach, "Analysis of airgap flux, current, and vibration signals as a function of the combination of static and dynamic airgap eccentricity in 3-phase induction motors," *IEEE Transactions on Industry Applications*, Vol. 33, No. 1, pp. 24-34, Jan. 1997.

[13] D. G. Dorrell, "Calculation of unbalanced magnetic pull in small cage induction motors with skewed rotors and dynamic rotor eccentricity," *IEEE Transactions on Energy Conversion*, Vol. 11, No. 3, pp. 483-488. Sep. 1996.

[14] Wang Tianyu, Wang Fengxiang, Bai Haoran, and Cui Hong, "Stiffness and critical speed calculation of magnetic bearing-rotor system based on FEA," *International Conference on Electrical Machines and Systems*, pp. 575-578, Oct. 2008.

[15] Yu Shenbo, Jiao Shi, Yuan Jing, and Zhao Yonghui, "Calculation of rotor critical speeds from permanent magnet synchronous machine," *International Conference on electrical and Control Engineering*, pp. 3439-3442. Jun. 2010.

[16] R. Belmans, W. Heylen, A. Vandenput, and W. Geysen, "Influence of rotor-bar stiffness on the critical speed of an induction motor with an aluminium squirrel cage," *IEEE Proceedings B Electric Power Applications*, Vol. 131, No. 5, pp. 203-208. Sep. 1984.

[17] Huang Jian, "Fault treatment of vibratoin caused by temperature rising in induction motor," *Huadian Technology*, Vol. 32, No. 11, pp. 44-49, Nov. 2010.

[18] E. Wiedemann, W. Kellenberger, *Construction of electrical machine*, Beijing, China machine press. Sep. 1976.

Qiang Lv He received the B.S. degree in 2011 in electrical engineering from Hefei University of Technology, Hefei, China. He joined the School of Electrical Engineering and Automation, Hefei University of Technology as a postgraduate. His main research interests are in the field of motor design, and finite element analysis.

Xiaohua Bao He received the B.S. degree in 1996, the M.Sc. degree in 2002 and the Ph.D. degree in 2008, all in electrical engineering from Hefei University of Technology, Hefei, China. He joined the School of Electrical Engineering and Automation, Hefei University of Technology and was promoted to Professor, in 2012. He was a visiting Scholar with Virginia Polytechnic Institute and State University, U.S. His main research interests are in the field of motor design, magnetic field analysis, and finite element analysis.

Yigang He He received the M.Sc. degree in electrical engineering from Hunan University, Changsha, China, in 1992 and the Ph.D. degree in electrical engineering from Xi'an Jiaotong University, Xi'an, China, in 1996. In 1990, he joined the College of Electrical and Information Engineering, Hunan University and was promoted to Associate Professor, Professor in 1996, 1999, respectively. From 2006 to 2011, he worked as the director of the Institute of Testing Technology for Circuits and Systems, Hunan University. He was a Senior Visiting Scholar with the University of Hertfordshire, Hatfield, U.K., in 2002. In 2011, he joined the Hefei University of Technology, China, and currently works as the Head of School of Electrical and Automation Engineering, Hefei University of Technology. His teaching and research interests are in the areas of circuit theory and its applications, testing and fault diagnosis of analog and mixed-signal circuits, electrical signal detection, motor measuring technology, analysis & calculation of electrical motor & electromagnetic fields, smart grid, radio frequency identification technology, and intelligent signal processing. He has published some 200 journal and conference papers in the aforementioned areas and several chapters in edited books. Dr. He has been on the Technical Program Committees of a number of international conferences. He was the recipient of a number of national and international awards, prizes, and honors.